Power Electronics and Drives
Volume 8(43), 2023 DOI: 10.2478/pead-2023-0020

Power Electronics and Drives

Optimisation of Model Predictive Torque Control Strategy with Standard and Multi-Objective Genetic Algorithms

Research paper

Emrah Zerdali[1,*], Aycan Gurel[2]

[1]*Ege University, Department of Electrical and Electronics Engineering, 35040 Izmir, Türkiye*
[2]*Niğde Ömer Halisdemir University, Department of Electrical and Electronics Engineering, 51200 Niğde, Türkiye*

Received: 04 June, 2023; Accepted: 22 August, 2023

Abstract: In this paper, the flux error-related weighting factor (WF) of the predictive torque control (PTC) strategy for induction motor (IM) control is optimised by a standard genetic algorithm (SGA) through speed errors only and multi-objective genetic algorithm (MOGA) through torque and flux errors. This paper compares the performances of both optimisation methods. Compared to MOGA, SGA offers a straightforward way to select WF and does not need a decision-making method to choose a final solution. But MOGA considers the given problem in a multi-objective way and directly optimises the control objectives of the PTC strate-gy. Comparisons are made over the flux and torque ripples, total harmonic distortion of stator phase current, and average switching frequency for different operating conditions. Simulation results show that both methods choose a close WF value. Consequently, SGA stands out in the optimisation of the PTC strategy with its simple structure.

Keywords: *Electric Drive System • Induction Motor • Model Predictive Control • Optimisation • Genetic Algorithm*

1. Introduction

Model predictive control (MPC) of power converters and electric drives is still open to research despite excessive development efforts (Rodriguez et al., 2022b, 2022a). In particular, finite control set MPC (FCS-MPC) strategies have been the focus of interest because of their compatibility with the discrete nature of power converters and the ease of incorporating additional control objectives (Li et al., 2022). Predictive torque control (PTC) and predictive current control (PCC) are the most popular ones and have been widely applied for high-performance induction motor (IM) control. In the literature, it is reported that PTC provides fewer torque ripples compared to PCC (Wang et al., 2015). However, both FCS-MPC strategies, particularly PTC in the presence of no additional control objectives, suffer from tuning the weighting factors (WFs) (Dragičević and Novak, 2019; Mamdouh et al., 2018).

One group of studies proposes different ways to select WFs, while the other group tries to eliminate these WFs. Considering the first group, the trial-and-error method is a well-accepted way to choose WFs in practice (Sahin et al., 2020). However, it is a tedious process and may not be possible to find optimal solutions, resulting in performance degradation. Instead, some researchers use meta-heuristic optimisation algorithms to optimise the WFs (Arshad et al., 2019; Davari et al., 2021; Guazzelli et al., 2019; Gurel and Zerdali, 2021a, 2021b; Wang et al., 2022; Zerdali, 2022). As with most of the current literature, Guazzelli et al. (2019) consider WF optimisation

* *Email: emrahzerdali@gmail.com*

as a multi-objective optimisation problem. For this purpose, they optimise the WFs by a multi-objective genetic algorithm (MOGA) using separate cost functions based on torque errors, flux errors, and total change in switching states. They also evaluate three different WFs from the Pareto set extensively. However, they do not propose a methodology for choosing a final solution among the Pareto set. This gap is filled by Arshad et al. (2019) who use the Technique for Order of Preference by Similarity to Ideal Solution (TOPSIS) decision-making method. Further analysis of the effect of different decision-making methods including TOPSIS is done by Gurel and Zerdali (2021a). It is concluded that a ranking-based decision-making (RDM) method provides better results in terms of torque and flux ripples, total harmonic distortion (THD) of stator phase current, and average switching frequency. The same decision-making method is used by Zerdali (2022), who optimises WF with MOGA using three different cost functions based on torque error, flux error and total change in switching states. Although this study considers the changes in switching states in the optimisation process, it ignores this additional control objective in the cost function of the PTC. Therefore, it only considers a single WF to optimise. In addition to all the studies that deal with the given problem as multi-objective, Gurel and Zerdali (2021b) and Davari et al. (2021) reduce this problem to a single-objective optimisation problem. Thus, they facilitate the optimisation phase by using a simpler algorithm and directly reaching the final solution. Gurel and Zerdali (2021b) use a standard genetic algorithm (SGA) and only speed errors to optimise the WF. Unlike all previous papers using offline meta-heuristic optimisation algorithms, Davari et al. (2021) and Wang et al. (2022) use these algorithms online. Davari et al. (2021) use an online simplified simulated annealing (SA) algorithm which use a single cost function consisting of torque and flux errors. Wang et al. (2022) extend the study proposed by Zerdali (2022) to multiple WFs. But they use a Gaussian distributed particle swarm optimisation (PSO) algorithm that uses a single cost function including different objectives. The approach used by Davari et al. (2021) and Wang et al. (2022), also known as the scalarisation method, is based on constructing a cost function from the weighted sum of several control objectives. Although both studies use equal weights, the scalarization method raises another problem caused by the determination of new WFs. However, meta-heuristic algorithms cannot adapt to the dynamic operating conditions of IM as they are not suitable for online optimisation due to their low convergence speeds and high computational loads.

This paper presents a comparison of PTC strategies optimised by an SGA and a MOGA. While many studies consider this optimisation problem in a multi-objective way, a very limited number of studies regard the given problem as a single-objective optimisation problem. To the best of the authors' knowledge, there is no study comparing these two points of view. For this purpose, the SGA in Gurel and Zerdali (2021b) and MOGA with RDM method in Gurel and Zerdali (2021a) have been selected to compare. Thus, this paper fills this gap by comparing both approaches in terms of control performance, design complexity, and computational complexity.

The rest of this paper is organized as follows. The PTC strategy for IM fed by a two-level voltage source inverter (2L-VSI) is presented in Section 2. Details on the optimisation of PTC strategy through standard and multi-objective GAs are provided in Section 3. To compare the resulting control performance of the optimised PTC strategies, various test results are presented in Section 4. Finally, a conclusion is given in Section 5.

2. Predictive Torque Control of Induction Motor

In this section, the dynamic model of IM driven by a 2L-VSI is first given and then the PTC strategy for IM control is introduced.

2.1. Dynamic Model of IM Driven by a 2L-VSI

The rotor flux-based discrete dynamic model of an IM motor is defined in the stator stationary axis reference frame ($\alpha\beta$ –) as follows (Zerdali et al., 2022):

$$\mathbf{x}_{k+1} = f(\mathbf{x}_k, \mathbf{u}_k) + \mathbf{w}_k \tag{1a}$$

$$\mathbf{z}_k = h(\mathbf{x}_k) + \mathbf{v}_k \tag{1b}$$

where $\mathbf{x}_k = \begin{bmatrix} i_{s\alpha,k} & i_{s\beta,k} & \psi_{r\alpha,k} & \psi_{r\beta,k} & \omega_{m,k} \end{bmatrix}^T$, $\mathbf{u}_k = \begin{bmatrix} u_{s\alpha,k} & u_{s\beta,k} \end{bmatrix}^T$, $h(\mathbf{x}_k) = \begin{bmatrix} i_{s\alpha,k} & i_{s\beta,k} & \omega_{m,k} \end{bmatrix}^T$, and

$$f(\mathbf{x}_k,\mathbf{u}_k)=\begin{pmatrix}\left(1-\frac{1}{T_\sigma}\right)i_{s\alpha,k}+\frac{k_r}{T_rL_\sigma}\psi_{r\alpha,k}+\frac{k_r}{L_\sigma}p_p\omega_{m,k}\psi_{r\beta,k}+\frac{1}{L_\sigma}u_{s\alpha,k}\\ \left(1-\frac{1}{T_\sigma}\right)i_{s\beta,k}+\frac{k_r}{T_rL_\sigma}\psi_{r\beta,k}-\frac{k_r}{L_\sigma}p_p\omega_{m,k}\psi_{r\alpha,k}+\frac{1}{L_\sigma}u_{s\beta,k}\\ \frac{L_m}{T_r}i_{s\alpha,k}+\left(1-\frac{1}{T_r}\right)\psi_{r\alpha,k}-p_p\omega_{m,k}\psi_{r\beta,k}\\ \frac{L_m}{T_r}i_{s\beta,k}+\left(1-\frac{1}{T_r}\right)\psi_{r\beta,k}+p_p\omega_{m,k}\psi_{r\alpha,k}\\ \frac{3}{2}\frac{p_p}{J_t}k_r\left(\psi_{r\alpha,k}i_{s\beta,k}-\psi_{r\beta,k}i_{s\alpha,k}\right)+\left(1-\frac{B_t}{J_t}\right)\omega_{m,k}-\frac{1}{J_t}\tau_{l,k}\end{pmatrix}.$$

In (1), f is the nonlinear function of states and inputs, h is the function of outputs, $\mathbf{x}_t$ is the state vector, $\mathbf{u}_t$ is the control input vector, $\mathbf{w}_t$ and $\mathbf{v}_t$ are zero-mean Gaussian distributed process and measurement noises, respectively. $i_{s\alpha}$ and $i_{s\beta}$ are the stator currents, $u_{s\alpha}$ and $u_{s\beta}$ are the stator voltages, $\psi_{r\alpha}$ and $\psi_{r\beta}$ are the rotor fluxes, ω_m is the angular mechanical speed, τ_l is the load torque applied to the shaft, J_t and B_t are the total inertia and viscous friction, respectively, p_p is the pole-pair. $T_\sigma = L_\sigma/R_\sigma$, $L_\sigma = L_s - L_m^2/L_r$, $R_\sigma = R_s + k_r^2 R_r$, $k_r = L_m/L_r$, and $T_r = L_r/R_r$, where R_s and R_r are stator and rotor resistances, respectively, L_s, L_r, and L_m are the stator, rotor, and mutual inductances, respectively.

When the stator terminals of IM are fed by a 2L-VSI, stator voltage vector ($\boldsymbol{u}_s = u_{s\alpha} + ju_{s\beta}$) is defined in terms of switching states $S_x \in \{S_a, S_b, S_c\}$ and dc-link voltage V_{dc} as follows:

$$\boldsymbol{u}_s = \frac{2}{3}V_{\mathrm{dc}}\left(S_a + \boldsymbol{a}S_b + \boldsymbol{a}^2 S_c\right) \tag{2}$$

where $S_x \in \{S_a, S_b, S_c\}$ indicates ON/OFF states of upper switches on each leg and $\boldsymbol{a}$ is the phase shift of 120 electrical degrees. $\boldsymbol{u}_s$ takes seven different values for eight switching combinations, called the finite control set. The inverter topology of the 2L-VSI and the possible voltage vectors are shown in Fig. 1.

2.2. PTC Strategy for IM Control

The PTC strategy uses a discrete system model to predict future system behaviour and a predefined cost function to choose the optimal voltage vector for the next control period. It requires stator or rotor flux information to predict stator flux, which is difficult and not efficient to measure. Therefore, an estimator/observer is often used to estimate it. A well-accepted way is to use the rotor current model, which is derived from the discrete dynamic IM model in (1), to estimate the rotor flux ($\boldsymbol{\psi}_r^e$) and then calculate the stator flux ($\boldsymbol{\psi}_s^e$) using the estimated rotor flux (Arshad et al., 2019; Davari et al., 2021; Guazzelli et al., 2019; Gurel and Zerdali, 2021a, 2021b; Wang et al., 2022; Zerdali, 2022).

$$\boldsymbol{\psi}_{r,k}^e = \boldsymbol{\psi}_{r,k-1}^e + T\left(R_r k_r \boldsymbol{i}_{s,k} - \left(\frac{1}{T_r} - j\omega_{r,k}\right)\boldsymbol{\psi}_{r,k-1}^e\right) \tag{3}$$

$$\boldsymbol{\psi}_{s,k}^e = k_r \boldsymbol{\psi}_{r,k}^e + L_\sigma \boldsymbol{i}_{s,k} \tag{4}$$

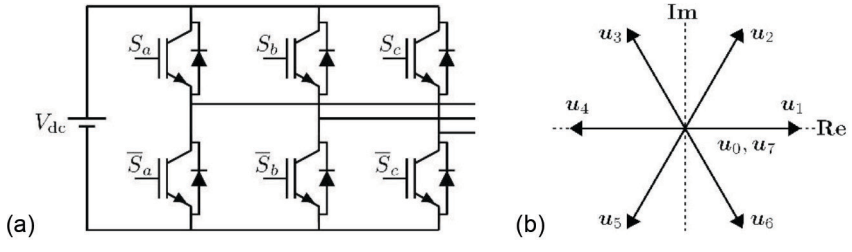

Fig. 1. 2L-VSI (a) Inverter topology (b) Possible voltage vectors.

Using (1) and (3), stator current (i_s^p) can be predicted as in (5). Also, stator flux (ψ_s^p) can be predicted as in (6) by substituting (4) into the voltage model of IM. Finally, the predicted electromagnetic torque (τ_e^p) is obtained using (5) and (6) as in (7) (Davari et al., 2021, Wang et al., 2015).

$$\boldsymbol{i}_{s,k+1}^{p}=\left(1-\frac{T}{T_{\sigma}}\right)\boldsymbol{i}_{s,k}+\frac{T}{T_{\sigma}R_{\sigma}}\left(k_r\left(\frac{1}{T_r}-j\omega_{r,k}\right)\boldsymbol{\psi}_{r,k}^{e}+\boldsymbol{u}_{s,k}\right) \tag{5}$$

$$\boldsymbol{\psi}_{s,k+1}^{p}=\boldsymbol{\psi}_{s,k}^{e}+T\left(\boldsymbol{u}_{s,k}-R_s\boldsymbol{i}_{s,k}\right) \tag{6}$$

$$\tau_{e,k+1}^{p}=1.5p_p\Im m\left(\left(\boldsymbol{\psi}_{s,k+1}^{p}\right)^{*}\left(\boldsymbol{i}_{s,k+1}^{p}\right)\right) \tag{7}$$

The main purpose of the PTC strategy is to control torque and flux, and it performs both controls using a predefined cost function which is constructed by the weighted sum of the torque and flux error terms. Since the PTC with this cost function cannot protect the electric drive from the overcurrents, an additional control objective I_m is often added to the cost function that protects the system from overcurrents. The resulting cost function is as follows:

$$g(j)=\lambda_{\tau}\left|\tau_e^{*}-\tau_{e,k+1}^{p}(j)\right|+\lambda_{\psi}\left|\left|\boldsymbol{\psi}_s^{*}\right|-\left|\boldsymbol{\psi}_{s,k+1}^{p}(j)\right|\right|+I_{m,k+1}(j), \tag{8}$$

where

$$I_{m,k+1}(j)=\begin{cases}0, & if\left(\left|\boldsymbol{i}_{s,k+1}^{p}(j)\right|\le i_{s,\max}\right)\\ \infty, & if\left(\left|\boldsymbol{i}_{s,k+1}^{p}(j)\right|> i_{s,\max}\right)\end{cases}. \tag{9}$$

In (8) and (9), λ_{τ} and λ_{ψ} are the weighting factors of torque and flux error terms, respectively, j represents the candidate voltage vector, and $i_{s,\max}$ is the maximum allowable limit of the stator current.

3. Optimisation of Predictive Torque Control

This section details the offline optimisation process of the PTC strategy by an SGA and a MOGA, respectively. For this purpose, the entire drive system shown in Fig. 2 has been implemented in MATLAB/Simulink and the Optimisation Toolbox in MATLAB has been used to optimise the PTC strategy because of its user-friendly environment. In addition, the λ_{τ} is assumed to be one, as in most papers in the literature. Therefore, this paper only focuses on optimising the λ_{ψ}.

3.1. Single Objective Optimisation with SGA

An SGA whose parameters are given in Table 1 is used to optimise the PTC strategy. This significantly simplifies the optimisation process by providing a single solution at the end of optimisation. Thus, necessity of choosing the final solution among the Pareto front solutions is eliminated. To optimise the WFs, the SGA needs a cost function with a single objective. For this purpose, a mean square error (MSE) value, defined as the difference between the reference and measured speeds, is used in this paper.

$$f_{\mathrm{SGA}}=\frac{1}{n}\sum_{i=1}^{n}\left(\omega_m^{*}-\omega_m\right)^2 \tag{8}$$

where n is the length of the data captured during the simulation period.

To eliminate the adverse effect caused by the random nature of the GAs, the optimisation process has been repeated 10 times for 20 generations and then a final solution has been chosen as 106.09 based on the analysis provided by Gurel and Zerdali (2021b). The corresponding boxplot illustration of the results for 20 repetitions is shown in Fig. 3.

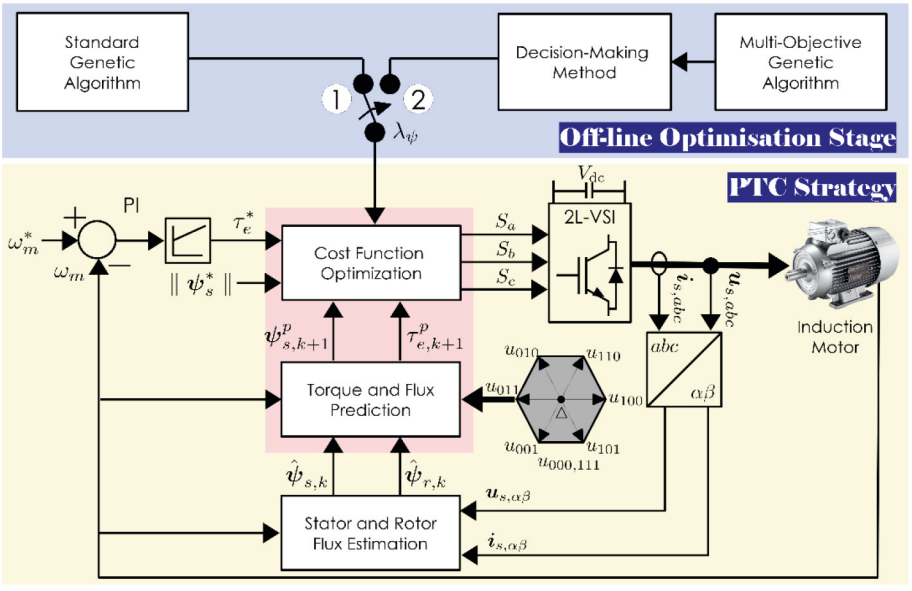

Fig. 2. Block diagram of the entire PTC-based IM drive system.

Algorithm	Parameter	Value	Parameter	Value
SGA	Population Size	30	Crossover Function	@crossoversinglepoint
	Max. Generation	20	Crossover Rate	0.8
	Lower Bound	1	Mutation Function	@mutationuniform
	Upper Bound	200	Mutation Rate	@tournament
MOGA	Population Size	50	Crossover Function	@crossovertwopoint
	Max. Generation	30	Crossover Rate	0.8
	Lower Bound	1	Mutation Function	@mutationadaptfeasible
	Upper Bound	200	Selection Function	@tournament
	Pareto Fraction	1	Tournament Size	2

Table 1. SGA and MOGA parameters used in optimisation process.

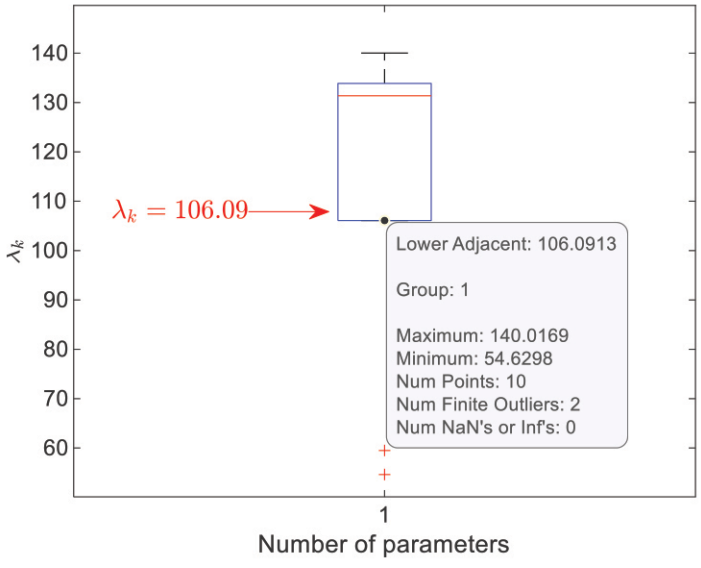

Fig. 3. MSE values with respect to the generations.

3.2. Multi Objective Optimisation with MOGA

MOGA with the parameters in Table 1 is used in this paper. Similar to the current literature, it uses the following two objective functions which include the MSE of torque and flux errors, respectively. Since it yields the Pareto set of optimal solutions, a final solution should be chosen among them. Based on the study proposed by Gurel and Zerdali (2021a), the RDM method is used in this paper.

$$f_{\mathrm{MOGA},1} = \frac{1}{n}\sum_{i=1}^{n}\left(\tau_e^* - \tau_e^p\right)^2 \tag{9a}$$

$$f_{\mathrm{MOGA},2} = \frac{1}{n}\sum_{i=1}^{n}\left(\left|\boldsymbol{\psi}_s^*\right| - \left|\boldsymbol{\psi}_s^p\right|\right)^2 \tag{9b}$$

After 30 generations, a Pareto set has been obtained as shown in Fig. 4. After applying the RDM method, a final solution has been chosen as 94.56.

4. Results

In this section, the PTC strategies optimised by SGA and MOGA are compared in terms of torque and flux ripples, average switching frequency, and total harmonic distortion (THD) of the stator current. To this end, a three-phase squirrel cage IM with the specifications in Table 2 is used. Simulation studies have been carried out with a sampling time frequency of 50 kHz. A proportional-integral (PI) controller with proportional and integral gains of 5 and 10, respectively, is used as the speed controller. The $i_{s,\max}$ is set to 15 A.

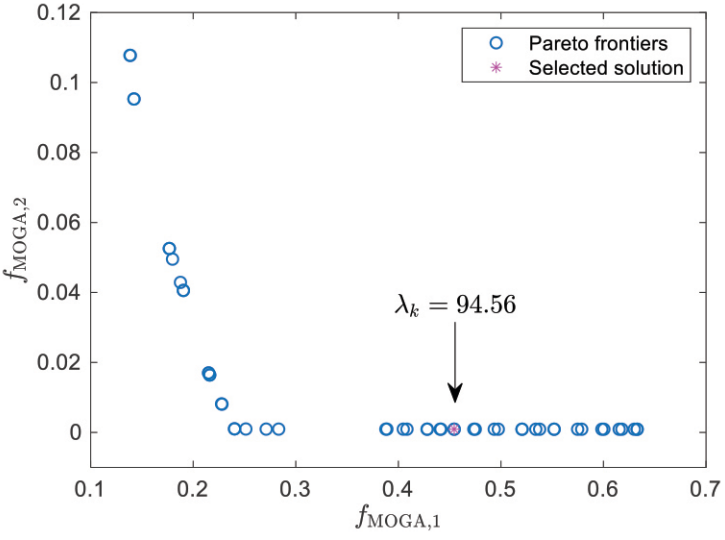

Fig. 4. Pareto set of optimal solutions obtained after multi-objective optimisation of the PTC strategy.

P	3 kW	R_s	2.283 Ω
V	380 V	R_r	2.133 Ω
I	6.9 A	L_m	0.22 H
f	50 Hz	L_s	0.2311 H
p_p	2	L_r	0.2311 H
n_m	1430 r/min	J_t	0.0183 kg.m^2
τ_l	20 Nm	B_t	0.001 N.m.s

Table 2. Specification of the IM used in the simulation studies.

Similar to previous papers, the following tests have been considered to compare the control performance of the optimised PTC strategies: 1) Operation at 5 rad/s under no-load and the rated load. 2) Operation at the rated speed under no-load and the rated load. 3) Speed reversal under rated load.

The resulting control performance for each test is presented in Figs. 5-7, respectively. To quantitatively support the graphical presentation, root mean square error (RMSE) and mean absolute error (MAE) values of flux, speed and torque are also provided in Table 3. Moreover, the quantitative results for percent flux and torque ripples, THD of stator phase current and average switching frequency are shown in Table 4. The mathematical expression of each performance index is as follows:

$$\chi_{\text{rip}} = \frac{\chi_{\max} - \chi_{\text{avg}}}{\chi_{\text{rated}}} \times 100 \tag{10}$$

where $\chi_{\max}$, χ_{avg}, and χ_{rated} indicate the maximum, average, and rated values of the dummy variable χ, respectively. In (10), χ represents torque or flux.

$$f_{\text{avg}} = \frac{N}{n_{sw} \times d} \tag{11}$$

where f_{avg} is the average switching frequency, N is the total state variations in power switches in the time interval of d seconds, n_{sw} is the number of power switches used in the power converter.

$$i_{\text{THD}} = 100 \times \sqrt{\left(\frac{I_{\text{rms}}}{I_{1,\text{rms}}}\right)^2 - 1} \tag{12}$$

where i_{THD} is the percentage THD of stator current for phase-*a*. I_{rms} and $I_{1,\text{rms}}$ are root mean square values of phase current and its fundamental component, respectively.

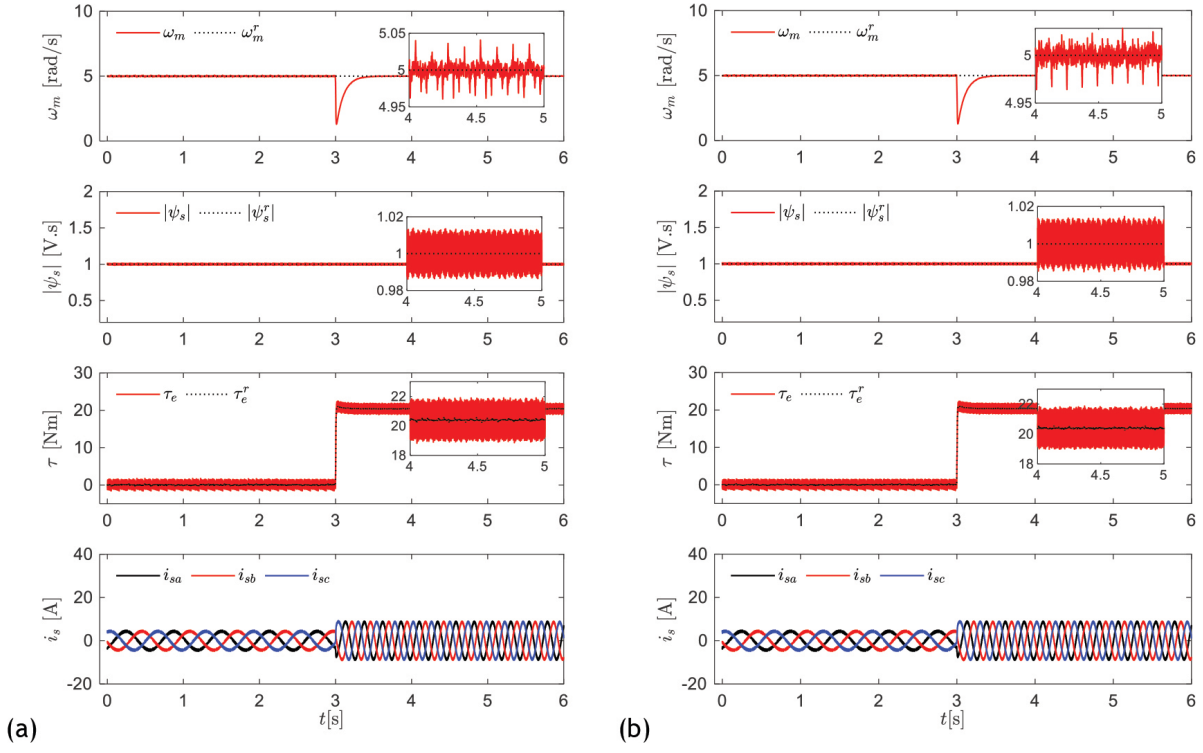

Fig. 5. Control performance at 5 rad/s under load changes (a) SGA ($\lambda_\psi = 106.09$) (b) MOGA ($\lambda_\psi = 94.56$).

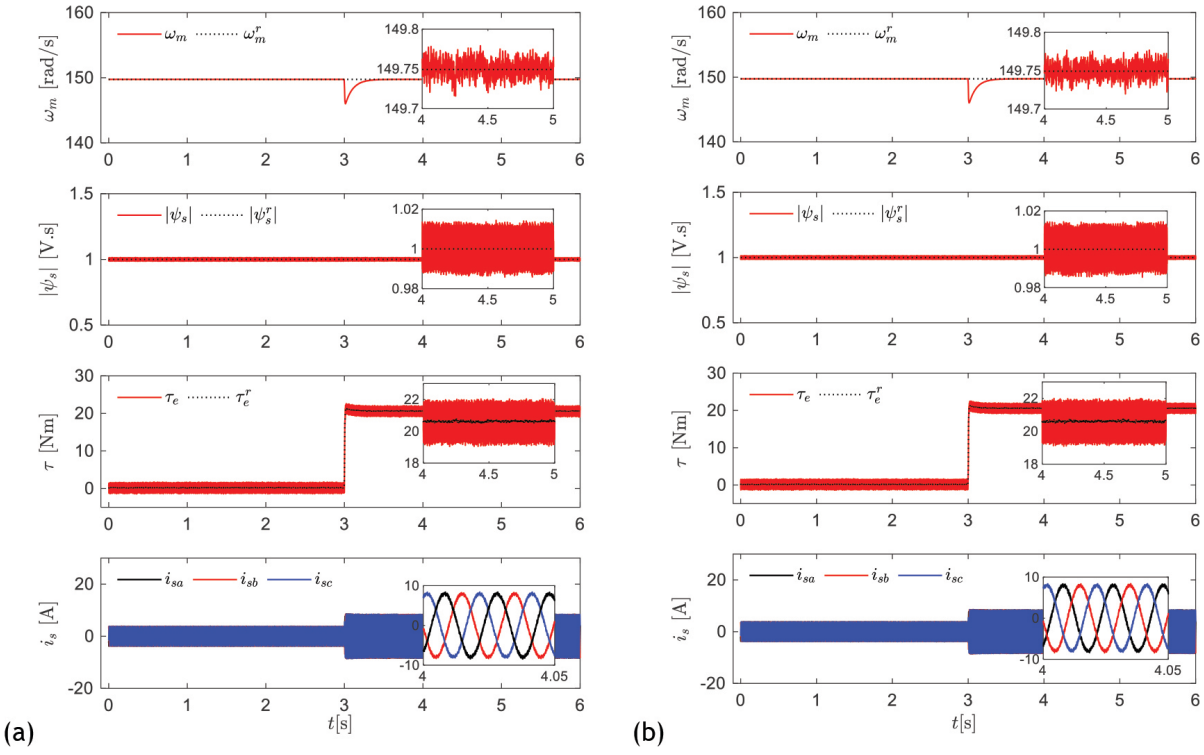

Fig. 6. Control performance at 150 rad/s under load changes (a) SGA ($\lambda_\psi = 106.09$) (b) MOGA ($\lambda_\psi = 94.56$).

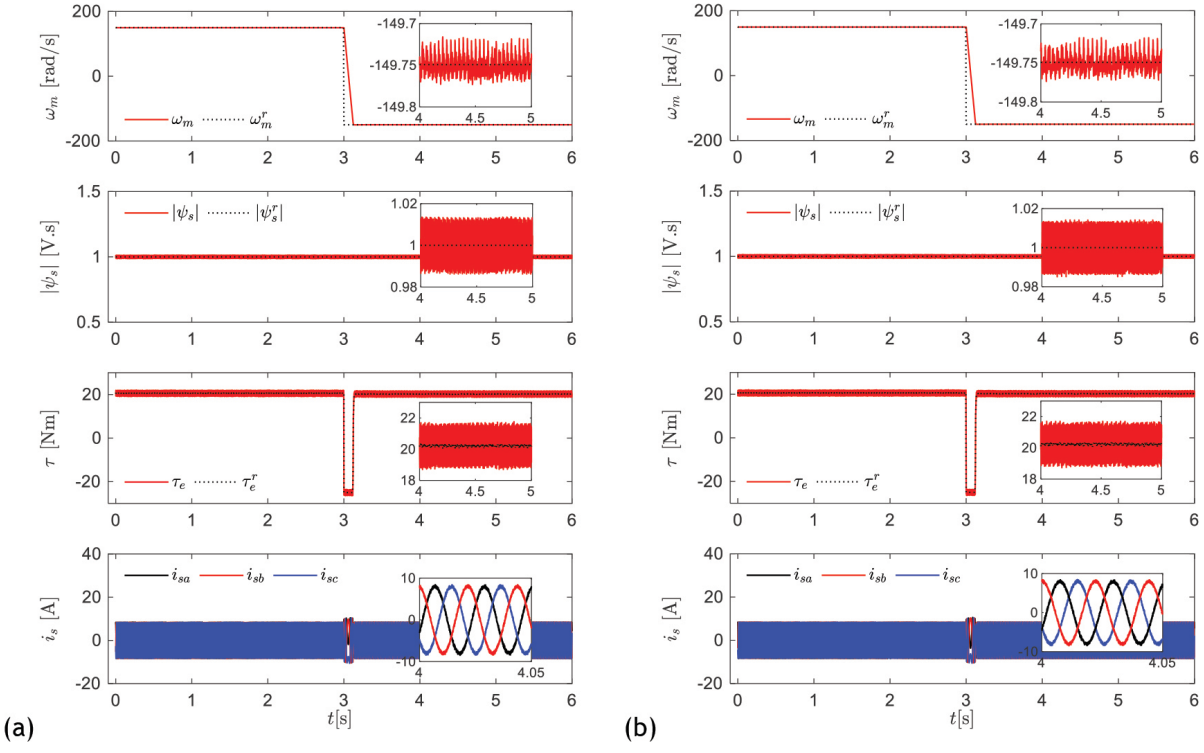

Fig. 7. Control performance under speed reversals at rated load (a) SGA ($\lambda_\psi = 106.09$) (b) MOGA ($\lambda_\psi = 94.56$).

		e_ω		$e_{\psi\|}$		e_τ	
	Method	RMSE	MAE	RMSE	MAE	RMSE	MAE
Fig. 5	Single Objective Optimisation	0.0011	0.0790	1.5815e-05	0.0045	0.0018	0.5267
	Multi Objective Optimisation	0.0011	0.0773	1.6356e-05	0.0047	0.0018	0.5126
Fig. 6	Single Objective Optimisation	0.0011	0.0742	1.6425e-05	0.0047	0.0019	0.5361
	Multi Objective Optimisation	0.0011	0.0736	1.6763e-05	0.0048	0.0018	0.5248
Fig. 7	Single Objective Optimisation	0.0615	2.6618	1.4850e-05	0.0046	0.0018	0.5382
	Multi Objective Optimisation	0.0615	2.6612	1.5149e-05	0.0047	0.0018	0.5274

Table 3. RMSE and MAE values for speed, flux and torque errors

Speed	Shaft Load	Method	$\psi_{\text{rip}}(\%)$	$\tau_{\text{rip}}(\%)$	$i_{\text{THD}}(\%)$	$f_{\text{avg}}(kHz)$
5 rad/s	No-Load	Single Objective Optimisation	1.4186	8.6703	4.22	0.494
		Multi Objective Optimisation	1.4210	7.5662	4.11	0.491
	20 Nm	Single Objective Optimisation	1.3444	7.7594	4.14	1.533
		Multi Objective Optimisation	1.4868	7.2441	4.17	1.632
150 rad/s	No-Load	Single Objective Optimisation	1.4649	7.8374	4.49	8.561
		Multi Objective Optimisation	1.5116	7.5986	4.34	8.641
	20 Nm	Single Objective Optimisation	1.3953	7.6556	4.23	9.215
		Multi Objective Optimisation	1.4434	7.2562	4.29	9.233

Table 4. Statistics on control performance of optimized weighting factors

Based on the results in Figs. 5-7 and the corresponding RMSE and MAE values in Table 3, it can be deduced that the WFs optimised by both approaches provide very close control performance. To take the comparison further, other performance indexes are needed. For this purpose, it is possible to use torque/flux ripples, THD of stator phase current, and average switching frequency. Table 4 presents the values of these additional performance indexes for some operating points.

Given the new performance indexes, SGA provides better flux ripples as it chooses a higher value than MOGA. As expected, this slightly increases torque ripples as flux errors dominate the cost function of the PTC at higher values of the WF. Also, SGA has a slightly lower average switching frequency for different operating conditions. As for the THD values of the stator phase current, there is a trade-off for both approaches. SGA provides higher THD values for both speeds at no load, but lower than MOGA at rated load.

Consequently, SGA is a strong candidate for the WF design of the PTC strategy due to its ease of application. However, this paper considers a single WF to optimise for comparison. In the case of multiple WFs, using SGA only with speed errors may be insufficient. Because it is difficult to relate speed errors to additional control objectives such as switching frequency reduction term.

5. Conclusion

In this paper, the flux error related WF of the PTC strategy has been optimised by SGA through speed errors and MOGA through flux and torque errors, and both optimised PTCs have been compared over their performances under different operating conditions. The simulation results show that both SGA and MOGA yield close WF values resulting in similar control performances. Consequently, SGA stands out compared to MOGA because it has a simple structure and eliminates the difficulty of choosing the final solution among the Pareto set. However, comparisons have been made for the PTC strategy with a single WF. In the case of multiple WFs, SGA using speed errors may be insufficient, as it is difficult to relate speed errors to other additional control objectives. In such a case, MOGA is still a strong candidate. Future studies will focus on comparing them in the presence of multiple WFs.

References

Arshad, M.H., Abido, M.A., Salem, A., Elsayed, A.H., 2019. Weighting Factors Optimization of Model Predictive Torque Control of Induction Motor Using NSGA-II With TOPSIS Decision Making. IEEE Access 7, 177595–177606. https://doi.org/10.1109/ACCESS.2019.2958415

Davari, S.A., Nekoukar, V., Garcia, C., Rodriguez, J., 2021. Online Weighting Factor Optimization by Simplified Simulated Annealing for Finite Set Predictive Control. IEEE Trans. Ind. Informatics 17, 31–40. https://doi.org/10.1109/TII.2020.2981039

Dragičević, T., Novak, M., 2019. Weighting Factor Design in Model Predictive Control of Power Electronic Converters: An Artificial Neural Network Approach. IEEE Trans. Ind. Electron. 66, 8870–8880. https://doi.org/10.1109/TIE.2018.2875660

Guazzelli, P.R.U., de Andrade Pereira, W.C., de Oliveira, C.M.R., de Castro, A.G., de Aguiar, M.L., 2019. Weighting Factors Optimization of Predictive Torque Control of Induction Motor by Multiobjective Genetic Algorithm. IEEE Trans. Power Electron. 34, 6628–6638. https://doi.org/10.1109/TPEL.2018.2834304

Gurel, A., Zerdali, E., 2021a. The Effect of Different Decision-Making Methods on Multi-Objective Optimisation of Predictive Torque Control Strategy. Power Electron. Drives 6, 289–300. https://doi.org/10.2478/pead-2021-0018

Gurel, A., Zerdali, E., 2021b. Metaheuristic Optimization of Predictive Torque Control for Induction Motor Control. Ömer Halisdemir Üniversitesi Mühendislik Bilim. Derg. 11, 55–61. https://doi.org/10.28948/ngumuh.969734

Li, T., Sun, X., Lei, G., Guo, Y., Yang, Z., Zhu, J., 2022. Finite-Control-Set Model Predictive Control of Permanent Magnet Synchronous Motor Drive Systems - An Overview. IEEE/CAA J. Autom. Sin. 9, 2087–2105. https://doi.org/10.1109/JAS.2022.105851

Mamdouh, M., Abido, M.A., Hamouz, Z., 2018. Weighting Factor Selection Techniques for Predictive Torque Control of Induction Motor Drives: A Comparison Study. Arab. J. Sci. Eng. 43, 433–445. https://doi.org/10.1007/s13369-017-2842-2

Rodriguez, J., Garcia, C., Mora, A., Davari, S.A., Rodas, J., Valencia, D.F., Elmorshedy, M., Wang, F., Zuo, K., Tarisciotti, L., Flores-Bahamonde, F., Xu, W., Zhang, Zhenbin, Zhang, Y., Norambuena, M., Emadi, A., Geyer, T., Kennel, R., Dragicevic, T., Khaburi, D.A., Zhang, Zhen, Abdelrahem, M., Mijatovic, N., 2022a. Latest Advances of Model Predictive Control in Electrical Drives - Part II: Applications and Benchmarking With Classical Control Methods. IEEE Trans. Power Electron. 37, 5047–5061. https://doi.org/10.1109/TPEL.2021.3121589

Rodriguez, J., Garcia, C., Mora, A., Flores-Bahamonde, F., Acuna, P., Novak, M., Zhang, Y., Tarisciotti, L., Davari, S.A., Zhang, Zhenbin, Wang, F., Norambuena, M., Dragicevic, T., Blaabjerg, F., Geyer, T., Kennel, R., Khaburi, D.A., Abdelrahem, M., Zhang, Zhen, Mijatovic, N., Aguilera, R.P., 2022b. Latest Advances of Model Predictive Control in Electrical Drives - Part I: Basic Concepts and Advanced Strategies. IEEE Trans. Power Electron. 37, 3927–3942. https://doi.org/10.1109/TPEL.2021.3121532

Sahin, I., Keysan, O., Monmasson, E., 2020. Experimental tuning and design guidelines of a dynamically reconfigured weighting factor for the predictive torque control of an induction motor, in: 2020 22nd European Conference on Power Electronics and Applications (EPE'20 ECCE Europe). IEEE, p. P.1-P.8. https://doi.org/10.23919/EPE20ECCEEurope43536.2020.9215739

Wang, F., Li, J., Li, Z., Ke, D., Du, J., Garcia, C., Rodriguez, J., 2022. Design of Model Predictive Control Weighting Factors for PMSM Using Gaussian Distribution-Based Particle Swarm Optimization. IEEE Trans. Ind. Electron. 69, 10935–10946. https://doi.org/10.1109/TIE.2021.3120441

Wang, F., Li, S., Mei, X., Xie, W., Rodríguez, J., Kennel, R.M., 2015. Model-based predictive direct control strategies for electrical drives: An experimental evaluation of PTC and PCC methods. IEEE Trans. Ind. Informatics 11, 671–681. https://doi.org/10.1109/TII.2015.2423154

Zerdali, E., 2022. Multi-objective weighting factor optimization of predictive torque controlled induction motor drive considering switching frequency, in: IV. International Turkic World Congress on Science and Engineering. Nigde, pp. 36–43.

Zerdali, E., Altintas, M., Bakbak, A., Mese, E., 2022. Computationally efficient predictive torque control strategies without weighting factors. Turkish J. Electr. Eng. Comput. Sci. 30, 2554–2567. https://doi.org/10.55730/1300-0632.3955